

## Reduction of Tip–Sample Contact Using Dielectrophoretic Force Scanning Probe Microscopy

Al M. Hilton, Brian P. Lynch, and Garth J. Simpson

*Anal. Chem.*, **2005**, 77 (24), 8008-8012 • DOI: 10.1021/ac051384k • Publication Date (Web): 09 November 2005

Downloaded from <http://pubs.acs.org> on March 23, 2009

### More About This Article

---

Additional resources and features associated with this article are available within the HTML version:

- Supporting Information
- Links to the 1 articles that cite this article, as of the time of this article download
- Access to high resolution figures
- Links to articles and content related to this article
- Copyright permission to reproduce figures and/or text from this article

[View the Full Text HTML](#)



# Reduction of Tip–Sample Contact Using Dielectrophoretic Force Scanning Probe Microscopy

Al M. Hilton, Brian P. Lynch, and Garth J. Simpson\*

Department of Chemistry, Purdue University, West Lafayette, Indiana 47907

Dielectrophoretic force microscopy is shown to allow for facile noncontact imaging of systems in aqueous media. Electrokinetic tip–sample forces were predicted from topography measurements of an interface and compared with experimental images. Correlation function and power spectral density analyses indicated that image feedback was maintained without mechanical contact using moderate potentials (e.g.,  $\sim 18$  nm off the surface for a 7-V<sub>pp</sub>, 100-kHz waveform). The applied dielectrophoretic force and the corresponding increase in effective tip radius were predictably adjusted by changing the peak potential.

The need to minimize probe–surface contact forces in atomic force microscopy (AFM) experiments has provided the stimulus for the development of several noncontact imaging techniques. Conventional forces required for stable feedback in AFM imaging ( $\sim 1$ – $5$  nN) can adversely affect the sample, the tip, or both in many applications.<sup>1</sup> Although standard intermittent contact imaging (e.g., tapping mode) techniques can reduce lateral forces on samples, the vertical forces at the point of contact can still be substantial enough to deform soft surfaces such as lipid membranes.<sup>2–5</sup> Forces of  $\sim 14$  nN have been shown to rupture the cellular membranes of erythrocytes.<sup>5</sup> Even if cell lysis does not occur, tip-induced stress on the cellular cytoskeleton may perturb some of the physiological functions of the cell.<sup>6</sup> Noncontact imaging can also significantly reduce adverse affects from short-range chemical interactions (e.g., from adhesion forces or from transfer of material from the surface to the tip or vice versa). In studies in which these short-range chemical interactions are the primary object of study (e.g., in studies of protein/receptor or antibody/antigen interactions), noncontact methods can allow for subsequent unbiased imaging with the same tip.<sup>7</sup> Finally, non-

contact techniques can be particularly important for protecting tips that can be easily damaged, such as near-field scanning optical microscopy probes.<sup>8</sup>

A variety of diverse methods are available for noncontact imaging of solid/air and solid/vacuum interfaces. However, a relatively small subset of these has been successfully applied for noncontact imaging under aqueous conditions. Arguably, the most common methods for noncontact imaging in liquids involve the detection of changes in the amplitude or phase of an oscillating probe (either vertically in the case of tapping mode<sup>9</sup> or horizontally in the case of dithering<sup>10</sup>), usually through hydrodynamic, electric, or magnetic interactions as a tip approaches a surface.<sup>2</sup> Unfortunately, these techniques are challenging in liquids due to the increased mechanical noise from Brownian motion and the reduction in the quality factor of the resonator from the high viscosity present at low Reynolds numbers. Because of these combined interactions, the forces required to generate detectable changes in the oscillation amplitude or phase of the probe in liquids are often too close to the noise floor of the instrument for facile noncontact imaging.<sup>11,12</sup>

Magnetic force microscopy has been demonstrated as an in situ method of imaging.<sup>12–14</sup> However, the most obvious limitation of magnetic force microscopy as a universal noncontact imaging technique is the requirement that the sample possess a permanent magnetic dipole, significantly limiting the classes of systems that can be investigated.

Direct current (and quasi-dc) electric forces have many appealing characteristics for noncontact imaging. Most notably, virtually all materials can be reasonably expected to exhibit a significant response in an electric field. Furthermore, the magnitude and sign of the force can be controlled in conventional electric force microscopy (EFM) experiments simply by changing the potential applied to the cantilever.<sup>2,15</sup> One significant drawback of standard electric force microscopy in studies of aqueous interfaces is the limited potential range available due to electrolysis of water.

\* To whom correspondence should be addressed. E-mail: gsimpson@purdue.edu.

- (1) You, H. X.; Lau, J. M.; Zhang, S.; Yu, L. *Ultramicroscopy* **2000**, *82*, 297–305.
- (2) Bonnell, D., Ed. *Scanning Probe Microscopy and Spectroscopy: Theory, Techniques, and Applications*, 2nd ed.; Wiley-VCH: New York, 2001.
- (3) Fan, T.-H.; Federov, A. G. *Langmuir* **2003**, *19*, 10930–10939.
- (4) Fan, T.-H.; Federov, A. G. *Langmuir* **2003**, *19*, 1347–1356.
- (5) Hategan, A.; Law, R.; Kahn, S.; Discher, D. E. *Biophys. J.* **2003**, *85*, 2746–2759.
- (6) Le Grimmelc, C.; Lesniewska, E.; Giocondi, M.-C.; Finot, E.; Vie, V.; Goudonnet, J.-P. *Biophys. J.* **1998**, *75*, 695–703.
- (7) Willemsen, O. H.; Snel, M. M. E.; van der Werf, K. O.; de Groot, B. G.; Greve, J.; Hinterdorfer, P.; Gruber, H. J.; Schindler, H.; van Kooyk, Y.; Figdor, C. G. *Biophys. J.* **1998**, *75*, 2220–2228.

- (8) Hsu, J. W. P. *Mater. Sci. Eng.* **2001**, *33*, 1–50.
- (9) Putman, C. A. J.; Vanderwerf, K. O.; Degrooth, B. G.; Vanhulst, N. F.; Greve, J. *Appl. Phys. Lett.* **1994**, *64*, 2454–2456.
- (10) Karrai, K.; Grober, R. D. *Appl. Phys. Lett.* **1995**, *66*, 1842–1844.
- (11) O'Shea, S. J.; Lantz, M. A.; Tokumoto, H. *Langmuir* **1999**, *15*, 5, 922–925.
- (12) Lantz, M. A.; O'Shea, S. J.; Welland, M. E. *Appl. Phys. Lett.* **1994**, *65*, 409–411.
- (13) Bai, J.; Saito, H.; Ishio, S. *J. Appl. Phys.* **2004**, *96*, 5924–5926.
- (14) Garcia-Martin, J. M.; Thiaville, A.; Miltat, J.; Okuno, T.; Villa, L.; Piroux, L. *J. Phys. D: Appl. Phys.* **2004**, *37*, 965–972.
- (15) Girard, P. *Nanotechnology* **2001**, *12*, 485–490.

Peak potentials are generally limited to less than 1.5 V. Since the mechanical force scales with the square of the electric field,<sup>16–18</sup> this limitation places significant restrictions on the dynamic range of the available forces. This restriction can be circumvented by using the native electric charge on an insulating tip to measure the local charge density of an aqueous interface, such as the electric double layer of a lipid bilayer.<sup>19,20</sup> However, the charge density on an insulating tip is difficult to accurately measure and control, which can complicate the interpretation of the image contrast and can limit the magnitude of the tip–sample electrostatic force.

In recent studies, a novel approach has been developed using radio frequency ac electric fields to perform dielectrophoretic force microscopy (DEPFM).<sup>21</sup> In DEPFM, complications arising from electrolysis are alleviated through the use of high-frequency (>100 kHz) waveforms, allowing access to a significantly greater dynamic range of forces than are available using analogous EFM approaches. Furthermore, DEPFM probes material properties (i.e., frequency-dependent electric polarizability) different from other established scanning probe techniques. In this paper, the non-contact aspects of DEPFM are explored in detail through direct comparison of theoretical and experimental DEPFM images of a rough porous silicon sample and through quantitative analysis of topographs obtained in the presence and absence of ac electric fields.

**Damped Driven Oscillator Model.** In tapping mode, the effect of the dielectrophoretic (DEP) force on the motion of a cantilever can be understood through a simple mechanical model. A damped, driven oscillator subjected to a spatially varying DEP force  $F_{\text{DEP}}$  is described by the following general equation.<sup>22</sup>

$$\frac{d^2z(t)}{dt^2} - \gamma \frac{dz(t)}{dt} + \frac{k}{m} z(t) + A_d \cos(\omega t + \phi_d) + F_{\text{DEP}}(z(t)) = 0 \quad (1)$$

In eq 1,  $z(t)$  is the time-dependent vertical displacement of the cantilever away from equilibrium in the absence of a DEP force,  $\gamma$  is the viscosity of the medium,  $k$  is the spring constant of the cantilever,  $m$  is the mass of the cantilever,  $A_d$  is the magnitude of the driving force,  $\omega$  is the angular frequency of the driving force, and  $\phi_d$  is the phase of the driving force.

The radius of the tip imposes a characteristic length scale describing the topographic feature sizes that will contribute most significantly to the DEP images. Large, rolling topographic features (relative to the effective tip radius) generate relatively small field gradients and DEP forces similar to those expected for a topographically flat sample. In the other limit, sharp features much smaller than the tip radius generate high local field

gradients, but collectively average to a minor net interaction. Maximum image contrast in DEPFM can be reasonably expected to arise when the curvature of the local surface is closely matched to the effective radius of curvature of the AFM tip.

From these arguments, an estimate of the DEP force arising from a rough conducting surface can be obtained from an analysis of the topography. The squared gradient of the topography [described by  $T(x,y)$ ] at each pixel of an image can be determined as follows.

$$\nabla^2 T(x,y) = \frac{1}{2} \left[ \frac{\partial^2}{\partial x^2} T(x,y) + \frac{\partial^2}{\partial y^2} T(x,y) + \frac{\partial}{\partial x} \frac{\partial}{\partial y} T(x,y) + \frac{\partial}{\partial y} \frac{\partial}{\partial x} T(x,y) \right] \quad (2)$$

Explicit numerical evaluation of the gradient using eight-connectivity digital topography gradients with a Sobel filter weighting<sup>23</sup> for a step size of  $h$  yields the following approximate expression for

$$\nabla^2 T_{x,y} \cong \frac{([6(x,y) - (x-h,y) - (x+h,y) - (x,y+h) - (x,y-h)]/h^2) / ([-[(x-h,y-h) + (x+h,y+h) + (x-h,y+h) + (x+h,y-h)]]/2h^2)}{2h^2} \quad (3)$$

Using eq 3, the squared gradient at each pixel of a discrete image can be calculated for a particular lateral distance  $h$  (in increments of the pixel size).

**Correlation Function Analysis.** The predicted DEP force map ( $P_{x,y}$ ) acquired from the topography using eq 3 ( $P_{x,y} \propto \nabla^2 T_{x,y}$ ) can be compared to the measured image ( $M_{x,y}$ ) using a simple cross-correlation function dependent on the step size,  $h$ .<sup>24</sup> In brief, each pixel in the predicted DEP image is multiplied by the corresponding measured DEP image and then averaged over all the accessible pixels in the images (eq 4).

$$C(h) = \sum_{x,y=0}^N \frac{P(h)_{x,y} M_{x,y}}{\sqrt{(P(h)_{x,y})^2 (M_{x,y})^2}} \quad (4)$$

If the two images are completely uncorrelated, the product of any two pixels is equally likely to be either positive or negative in sign (since the average height is zero), and the value of the correlation function  $C(h)$  will average to zero. Conversely, two identical images will yield a correlation function value equal to unity. The function  $C(h)$  should not be confused with a 1D or 2D spatial cross-correlation function, in which the correlation between two images is compared as a function of spatial shift. In eq 4,  $C(h)$  describes the correlation between the measured DEP force map and the theoretical DEP force maps, calculated from the gradient of the measured topography. The gradient of a real surface depends sensitively on the length scale  $h$  over which it is

(16) Hu, J.; Xiao, X.-D.; Salmeron, M. *Appl. Phys. Lett.* **1995**, *67*, 476–478.  
 (17) Luna, M.; Rieutord, F.; Melman, N. A.; Dai, Q.; Salmeron, M. *J. Phys. Chem. A* **1998**, *102*, 6793–6800.  
 (18) Inoue, T.; Ogletree, D. F.; Salmeron, M. *J. Vac. Sci. Technol. B* **2001**, *19*, 675–682.  
 (19) Johnson, A. S.; Nehl, C. L.; Mason, M. G.; Hafner, J. H. *Langmuir* **2003**, *19*, 10007–10010.  
 (20) Rotsch, C.; Radmacher, M. *Langmuir* **1997**, *13*, 2825–2832.  
 (21) Lynch, B. P.; Hilton, A. M.; Doerge, C. H.; Simpson, G. J. *Langmuir* **2005**, *21*, 1436–1440.  
 (22) Finney, R. L.; Ostberg, D. R. *Elementary Differential Equation with Linear Algebra*; Addison-Wesley: Reading, MA, 1976.

(23) Sobel, I. Stanford University Artificial Intelligence Lab: Palo Alto, CA, 1970.  
 (24) Dost, M.; Vogel, D.; Winkler, T.; Vogel, J.; Erb, R.; Kieselstein, E.; Michel, B. In *Nondestructive Detection and Measurement for Homeland Security*; Doctor, S. R., Bar-Cohen, Y., Aktan, A. E., Eds.; International Society for Optical Engineering (SPIE): Bellingham, WA, 2003.

calculated.<sup>25–27</sup> The correlation function in eq 4 describes the agreement between the predicted and measured DEP force maps as a function of this characteristic distance  $h$ .

A maximum in the correlation function in eq 4 is expected when surface features are comparable in scale to a characteristic length scale  $\Delta R_{\text{eff}}$ , equal to the change in effective radius of curvature of the tip. The topograph is already a convolution of a tip with radius  $\sim 40$  nm. The addition of the field-induced force results in preferential enhancement of features with size scales comparable to the effective tip radius. If these measurements are truly noncontact, the effective tip radius is expected to increase with increasing ac potential.

**Experimental Methods.** A detailed description of the DEPFM instrumentation has been described elsewhere.<sup>21</sup> Briefly, a Dimension 3100 atomic force microscope (Veeco) was modified to allow for an ac potential to be applied between the AFM cantilever and a grounded underlying semiconductive silicon substrate with a thin oxide overlayer. A porous silicon film was created through electrochemical HF etching (*Caution: HF is highly corrosive*), resulting in a surface having an rms roughness of 6–10 nm at a  $1 \mu\text{m} \times 1 \mu\text{m}$  scan size.<sup>28</sup> The waveform output of a function generator was applied across the tip and the substrate on alternating scan lines of the acquired images. In this way, complementary images were acquired in the presence and absence of an applied field during each complete raster pattern. Interpolation and subtraction of each pair of alternate line images yielded a corresponding DEP force map in which the image contrast was attributed to changes in the tip–surface DEP forces. Imaging in all DEPFM experiments was performed in tapping mode in high resistivity ( $\sim 17 \text{ M}\Omega \text{ cm}$ ) water (NANOpure, Barnstead/ThermoLyne Corp.) with titanium/platinum-coated silicon nitride AFM cantilevers ( $\mu\text{Masch}$ ) having spring constants of  $\sim 1 \text{ N/m}$  and typical resonance frequencies of 6–8 kHz in water. Power spectral density (PSD) plots were acquired using the instrument control software (Veeco). The same raw images were used in both the correlation function and PSD analyses.

**Electrostatic Calculations.** The overall magnitude and functional form of  $F_{\text{DEP}}$  in eq 1 dictate the contrast observed in the DEP images. For a topographically rough conducting (or semiconducting) interface, analytical expressions for  $F_{\text{DEP}}$  are nontrivial to generate. However, the limiting case of a topographically flat surface can yield qualitative insights. At short separations  $d$  between the tip and the surface for a flat conducting substrate (Figure 1), the tip can be approximated as a locally flat conductor, giving a  $1/d$  distance dependence for the force (consistent with previous experiments and calculations).<sup>29</sup> At length scales much greater than the tip radius, the tip can be treated as a point source. In this limiting case, a  $1/d^2$  relationship emerges, consistent with the force between a point charge and its image dipole.<sup>30</sup> From consideration of these limiting cases, it is reasonable to expect that the DEP forces arising from a tip at close contact to a

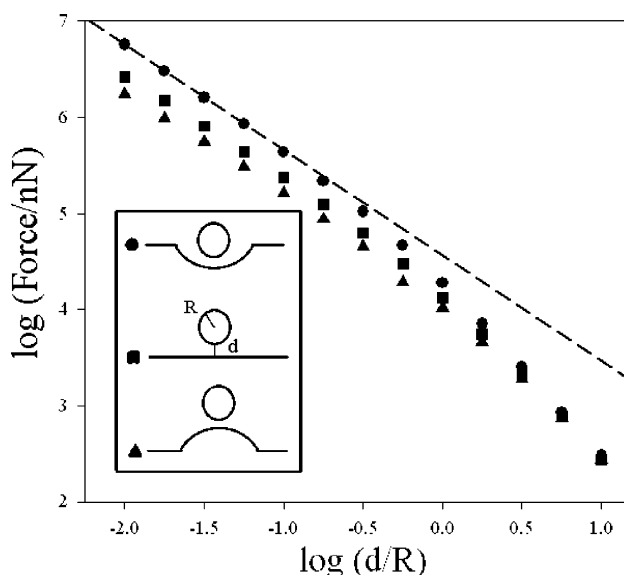


**Figure 1.** Electrostatic calculations of the vertical force on a conducting sphere adjacent to a conducting surface as a function of the separation between the two surfaces. The distance is expressed as a unitless ratio normalized to the effective radius of curvature of the tip ( $d/R$ ). Calculations were performed for surfaces exhibiting convex (triangles), concave (circles), and flat (squares) features (see inset). The dashed line indicates a slope of  $-1$ , corresponding to a  $1/d$  dependence.

topographically rough surface will scale approximately inversely with distance and will approach inverse quadratic behavior with increasing distance. However, the shape of the conducting substrate will likely have a strong effect on the electric field at short distances, suggesting that DEPFM can be reasonably expected to exhibit a strong sensitivity to local surface curvature.

To understand the effect of local curvature on DEPFM image feedback, a series of model systems were analyzed using a finite element analysis program (Maxwell 3D Field Simulator, Ansoft Corp.). In these calculations, a charged spherical conductor (approximating an AFM tip) was placed at varying distances above topographically flat surfaces exhibiting either concave or convex features comparable in dimension to the tip radius (Figure 1). Consistent with expectations, calculations for a flat surface recovered a  $1/d$  dependence at short length scales that approached a  $1/d^2$  dependence at increasing distance. The convex surface features yield a smaller DEP force and a shallower distance dependence than the concave surface at similar tip–sample separations, presumably because of differences in the longer range interactions with the extended surface.

Inserting the calculated magnitudes and distance dependences expected for convex versus concave topographic features into eq 1 yielded a prediction of greater damping of the cantilever amplitude for convex features. This initially paradoxical trend (concave features generate greater predicted DEP forces with steeper distance dependences, but lead to lesser damping) can be understood by considering the mechanism of image feedback. A steeper distance dependence results in less sensitivity in tapping mode imaging, presumably because the force acts preferentially on a smaller portion of the cycle during the cantilever oscillation. Consequently, “bumps” in topography are predicted to correlate with increased apparent DEP force as measured by the instrument.

(25) Simpson, G. J.; Rowlen, K. L. *Chem. Phys. Lett.* **1999**, *309*, 117–122.

(26) Simpson, G. J.; Rowlen, K. L. *J. Phys. Chem. B* **1999**, *103*, 3800–3811.

(27) Simpson, G. J.; Rowlen, K. L. *J. Phys. Chem. B* **1999**, *103*, 1525–1531.

(28) Lee, E. J.; Bitner, T. W.; Ha, J. S.; Shane, M. J.; Sailor, M. J. *J. Am. Chem. Soc.* **1996**, *118*, 5375–5382.

(29) Sacha, G. M.; Verdager, A.; Martinez, J.; S\_nz, J. J.; Ogletree, D. F.; Salmeron, M. *Appl. Phys. Lett.* **2005**, *86*, 123101–123103.

(30) Jackson, J. D. *Classical Electrodynamics*, 2nd ed.; John Wiley & Sons: New York, 1975.

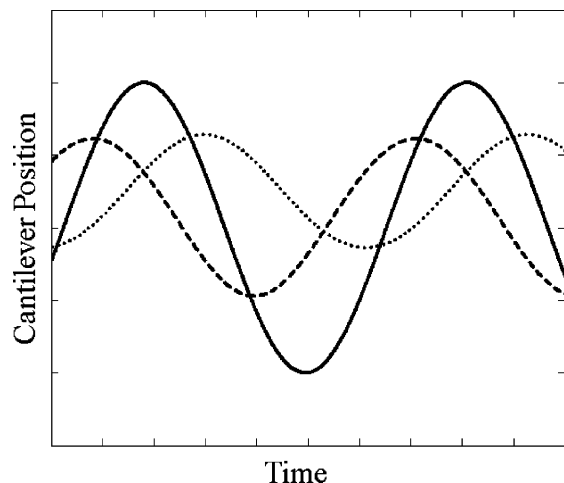


**Figure 2.** Calculated amplitude of an oscillating cantilever in the absence of an applied ac potential (solid) and in the presence of attractive (dashed) and repulsive (dotted) DEP forces.

A series of measurements was performed to compare the instrument response with predictions using the simple-damped driven oscillator model described by eq 1. Calculations of the predicted change in the amplitude and phase of the cantilever motion in the presence of a spatially varying DEP force are shown in Figure 2. Both the amplitude and phase of the cantilever oscillation are affected by the DEP force. When driven at the resonant frequency, either attractive or repulsive DEP forces dampen the amplitude oscillation, which is recorded experimentally as an increase in apparent height (i.e., the tip/sample distance is increased in order to maintain a constant amplitude of oscillation). In the present studies, it can be reasonably assumed that the DEP forces will be exclusively attractive given the substantial differences in conductivity between silicon and ultrapure water.

Figure 3 contains images of the topography, the predicted DEP force map, and the measured DEP force map for a  $250 \text{ nm} \times 250 \text{ nm}$  region of a porous silicon sample. Qualitatively similar images were obtained at different scan sizes. Topographs similar to those shown in Figure 3a indicate a surface with an rms roughness of  $9 \text{ nm}$  ( $\pm 2 \text{ nm}$ ) over a  $1 \mu\text{m} \times 1 \mu\text{m}$  scan size. Inspection of the DEP force map indicates increased cantilever damping for convex features and reduced damping for concave features.

**Correlation Function Analysis.** Quantitative topographic analysis combined with eq 4 allowed for the prediction of the anticipated DEP image expected from porous silicon. Assuming a rough conducting (or semiconducting) substrate with a thin insulating overlayer, the length scale  $h$  over which the gradient was calculated is the only adjustable parameter in eq 4. To determine the optimized characteristic length scale  $\Delta R_{\text{eff}}$  of the surface features contributing to the measured DEP forces (expected to be approximately equal to the effective change in the radius of curvature of the tip), correlation functions between the normalized predicted and measured DEP force maps over a range of values for  $h$  were determined using eq 4, after first subtracting the native correlation of the topography with itself (i.e., the  $0 \text{ V}_{\text{pp}}$  result). The resulting values of  $\Delta R_{\text{eff}}$  obtained from the maxima of the correlation functions  $C(h)$  were consistent over four image sizes ranging from  $250 \text{ nm} \times 250 \text{ nm}$  to  $2 \mu\text{m} \times 2 \mu\text{m}$  (not shown). The measured values of  $\Delta R_{\text{eff}}$  from the maxima in Figure 4 change significantly upon application of the DEP force. At a 100-kHz

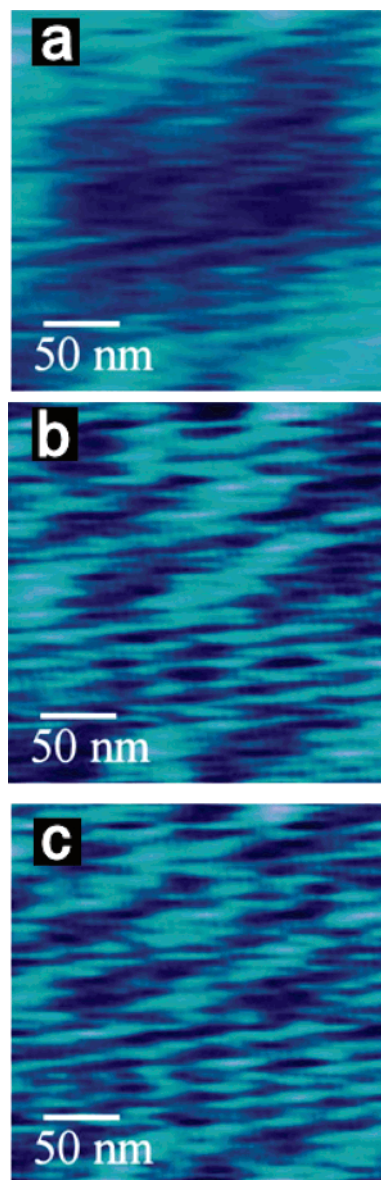


**Figure 3.** Topograph of a  $250 \text{ nm} \times 250 \text{ nm}$  porous silicon sample (a), an experimentally measured DEP force map (b) of the same sample (100-kHz,  $7\text{-V}_{\text{pp}}$  potential), and predicted DEP image (c) calculated from the topography in (a). The vertical range of the topograph is  $\sim 50 \text{ nm}$ , while the DEP images are in relative units of force (normalized to the maximum force).

potential of  $7 \text{ V}_{\text{pp}}$ , the DEP forces were sufficient to yield a value of  $\Delta R_{\text{eff}} = 18 \text{ nm}$ . Increasing the peak potential resulted in a roughly quadratic increase in  $\Delta R_{\text{eff}}$ .

**Power Spectral Density Analysis.** A complementary measurement of the increase in effective tip radius was obtained through the analysis of power spectra of the topographic images acquired in the presence and absence of DEP forces. When a surface is imaged with an AFM probe, the acquired image is a convolution of the shape of the AFM tip and the actual shape of the scanned object. The PSD of a surface shows a relative decrease in high-frequency contributions when imaged with a dull tip as compared to a PSD imaged with a sharp tip.<sup>31</sup> When an object is

(31) Fang, S. J.; Haplepete, S.; Chen, W.; Helms, C. R. J. *Appl. Phys.* **1997**, *82*, 5891–5898.

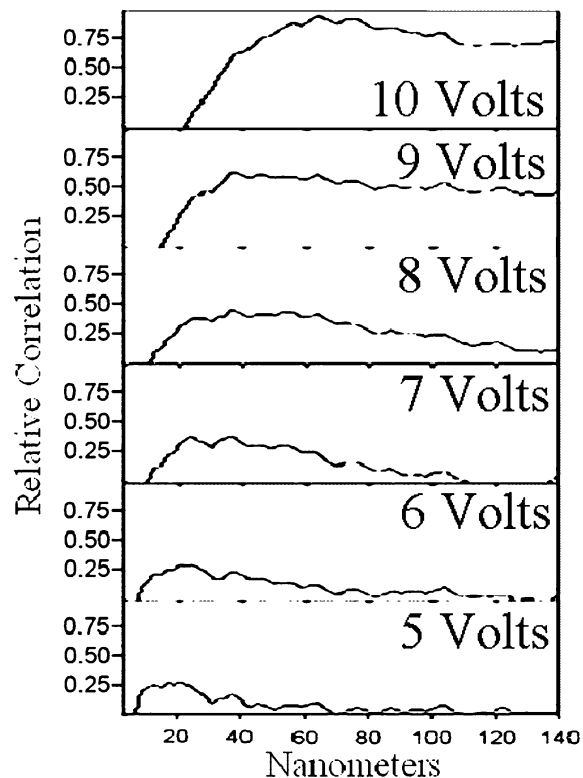


**Figure 4.** Correlation functions of the measured and predicted DEP force maps as a function of length scale  $h$  for a  $1\ \mu\text{m} \times 1\ \mu\text{m}$  porous silicon/water interface at several applied peak potentials, calculated using eq 4.

imaged with an AFM probe, the acquired image is a convolution of the shape of the AFM tip and the actual shape of the scanned object. The measured power of the high spatial frequency components of the image PSD are consequently intimately dependent on the effective radius of curvature of the scanning probe tip.

PSD analyses were performed for images acquired in the presence and absence of a 100-kHz ac electric field in order to determine the field-induced changes in the spatial frequency contributions. A representative PSD plot of the change in the spectral power in the presence of a DEP force is shown in Figure 5. Comparison of the PSDs for porous silicon images acquired in both the presence and absence of an ac electric field revealed a preferential loss in the high spatial frequency elements in the DEPFM images. These trends were reproducible over multiple images and multiple scan sizes. Superimposed in Figure 5 is the value of the effective increase in tip radius obtained by correlation function analysis.

The PSD plot in Figure 5 indicates that the effective radius of curvature increased significantly upon application of the ac field. The spatial frequencies preferentially removed in the presence of the DEP force (i.e., with periods less than  $\sim 20$  nm) are in remarkably good agreement with the measured increase in effective tip radius from the correlation function analysis (i.e.,  $\sim 18$  nm). Taken together, these collective data suggest that the DEPFM imaging technique is able to maintain feedback in tapping mode operation under aqueous conditions without mechanically

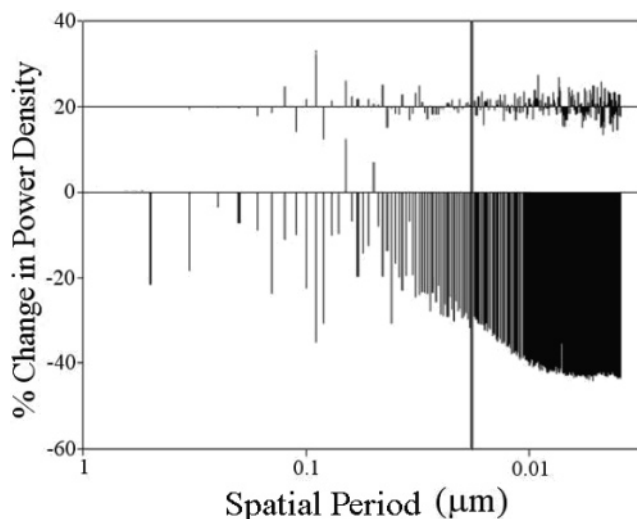


**Figure 5.** Relative change in PSD for a  $1\ \mu\text{m} \times 1\ \mu\text{m}$  porous silicon/water DEPFM image after the application of a 100-kHz, 7- $V_{pp}$  potential. The value of the effective increase in tip radius of 18 nm obtained by correlation function analysis is shown as a vertical line. A control measurement with a 0  $V_{pp}$  potential (offset by +25%) is also shown.

contacting the sample surface. The forces driving this novel noncontact imaging approach can be easily tuned by simple changes to the applied ac potential.

In summary, correlation function analysis and PSD measurements support the noncontact nature of DEPFM under aqueous conditions. Using a theoretical treatment based on finite element analysis, ac electrokinetic forces were predicted from topography measurements of a porous silicon/water interface. The predicted DEPFM images generated exclusively from the topography were compared with those measured experimentally using a correlation function technique, the results of which yielded excellent quantitative agreement between theory and experiment. The correlation function approach also allowed direct measurement of the increase in effective radius upon application of the DEP force. The results obtained from the correlation function analysis agreed quantitatively with independent measurements of the changes in power spectral density from topography measurements acquired in the presence and absence of the ac electric field. The development of reliable noncontact imaging approaches that are applicable under aqueous conditions is particularly significant for studies of biological interfaces, in which the forces required for traditional imaging often substantially perturb the sample under study.

#### ACKNOWLEDGMENT

The authors gratefully acknowledge financial support from the Showalter Trust Organization, the American Chemical Society Petroleum Research Fund (Type G), Eli Lilly (New Untenured Faculty Award), and the Sloan Foundation. We also acknowledge assistance from Christopher Doerge and the Jonathon Amy Facility for Chemical Instrumentation.

Received for review August 3, 2005. Accepted October 6, 2005.

AC051384K